Srivas, P. K., Kapat, K., Chaitanya, K., Koley, S., Su, B., & Dhara, S. (2021). Net shape forming of Ti6Al4V implants via green machining. *Journal of Materials Research*, *36*(19), 3905-3913. https://doi.org/10.1557/s43578-021-00360-w

Net Shape Forming of Ti6Al4V implants via Green Machining

Pavan Kumar Srivas[1], Kausik Kapat[1¥], Krishna Chaitanya S[1¥], Subhranil Koley[1], Bo Su[2], Santanu Dhara[1,*]

[1]School of Medical Science and Technology, Indian Institute of Technology Kharagpur, West Bengal, India 721302

[2]Biomaterials Engineering for Biological and Medical Applications, University of Bristol, UK

*Corresponding author e-mail address: sdhara@smst.iitkgp.ac.in

[¥-]These authors contributed equally

Abstract

Machining of bulk Ti6Al4V is relatively difficult owing to low elastic modulus, high work hardening tendency, stickiness, poor thermal conductivity besides formation of long continuous chips during machining. Near net shaping through green machining could be a viable alternative to conventional milling procedure. Herein, fabrication of Ti6Al4V dental root and spinal plate equivalents was successfully demonstrated through machining of green Ti6Al4V compacts prepared by plastic dough processing (PDP). For process reliability, the green as well as the sintered components were characterized for physico-mechanical properties, defect and shrinkage analysis for dimensional accuracy of the desired objects and Weibull modulus study for ensuring reliability of mechanical properties of the samples. Evidently, green machining could be a simple viable alternative for manufacturing of titanium implants in a cost-effective way.

Keywords: Metal machining, powder metallurgy, cost-effective, extrusion, sintering

1. Introduction

Titanium and its alloys are widely used for dental and orthopedic applications under load-bearing conditions owing to their high specific strength, fatigue resistance, excellent biocompatibility and osteo-conductivity [1, 2]. Titanium processing through powder metallurgy route is a preferred choice over melt casting mainly due to high infrastructural requirement and investment associated with its high melting point and oxygen sensitivity. Gelcasting or slurry-based technique, originally developed for ceramics powder processing, is little explored for manufacturing of titanium components. However, gelcasting of metal powder was not paid much attention due to several challenges including high settling rate, usage of excessive binder and thickener along with structural defects like inhomogeneity, residual porosities, coarse microstructure and low fatigue strength [3, 4]. In earlier study, we proposed a novel powder processing technique, i.e., plastic dough processing (PDP) for shape fabrication using both fine and coarse metal powders under ambient condition [5, 6]. The process is highly versatile over gelcasting in terms of very low process cycle, easy formability, homogeneous particle distribution, low drying shrinkage and uniform microstructure for both dense and porous shapes. Machining of bulk titanium encounters difficulty for its poor thermal conductivity, low Young's modulus, high sticking tendency and work hardening [7-12]. Poor thermal conductivity of titanium may also lead to accumulation of frictional heat at tool-work piece interface [12], whereas machining leads to work hardening necessitating high machining force thereby affecting tool life [13, 14] as well as phase transformation of Ti6Al4V [15, 16]. Therefore, appropriate heat dissipation technique (e.g., usage of liquid nitrogen and other coolants) and machining tools with high heat conductivity are necessary to overcome these issues [17]. In this direction, Wang *et al.* (1998) and Lei *et al.* (2002) developed self-propelled as well as driven rotary tools for

machining of Ti6Al4V; in this way, cutting temperature was greatly reduced without any negative influences on material removal rate [18, 19]. Moreover, sophisticated tools, e.g., cemented carbide (WC/Co), cubic-boron-nitride (CBN), polycrystalline diamond, and polycrystalline boron nitride tools were also developed with advantage of high heat and chemical stability for better performance [20-25]. Noteworthy that carbide- and diamond- coated tools performed better for Ti6Al4V machining compared to uncoated- as well as CBN tools. Undoubtedly, usage of such sophisticated tools or coolant imposes additional cost to the process.

Samples prior to sintering, i.e., green bodies, possess significantly lower strength and hardness compared to the bulk and sintered objects. Recently, green machining is more emphasized to minimize energy consumption as well as dependence on expensive tools and coolants required for bulk machining [26]. The aim of the present study was to develop a viable green machining approach for cost-effective fabrication of customized Ti6Al4V shapes via powder metallurgy route. Accordingly, the study anticipated the following objectives (a) preparation of dough using Ti6Al4V powder, binder, additives and solvent using a proprietary process [5, 6]; shape prefabrication through rolling and extrusion (b) developing software models for dental roots and spinal plate equivalents by Solidworks®; based on that green machining of prefabricated shapes using a computer numerical control (CNC) machine and custom-designed diamond particle embedded pointed end tool [27], (c) finally, characterization of sintered machined objects for physico-mechanical properties, analyzing defects as well as shrinkage for dimensional accuracy of the desired objects, Weibull modulus study to ensure process viability based on reliability of mechanical properties. Based on evidences, green machining could be established as a cost-effective sustainable alternative for developing titanium-based implants.

2. Results and discussion

2.1 Dough preparation and shape prefabrication

The highly viscous dough prepared by high shear mixing of Ti6Al4V powder-polymer-solvent blend following an established procedure [5, 6] was extruded and pressed into rods and sheets, respectively and subjected to vacuum drying. The dried green samples exhibited a smooth appearance without any visual defects and found to possess 66% ± 1.7% green density matching the theoretical value necessary for achieving > 97% sintered density. The sintered samples exhibited ~15% linear shrinkage, matching with the values reported in our earlier study [28].

2.2 Tool design and green machining

Diamond impregnated conical pointed end tool was employed for machining of green Ti6Al4V samples. As per the 3D design, Ti6Al4V based net shaped green bodies resembling dental root and spinal plate were successfully machined using 'stl' files. Machining parameters such as depth of cut, linear velocity and rpm of the tool (as mentioned in Table 1) previously optimized for green machining of alumina compacts [27] were also applicable for green machining of Ti6Al4V compacts.

Table 1: Parameters for machining green Ti6Al4V

Parameters	Surfacing	Roughing	Finishing
X/Y speed (mm/s)	3	3	3
Z speed	3	3	3
Spindle speed (rpm)	8000	8000	8000
Path interval (mm)	0.2	0.2	0.1
Depth of cut (mm)	1.0	1.0	0.1

Accordingly, surfacing and roughing operations were carried out at optimal speeds, X-Y-Z linear movement at 3 mm/s and spindle speed at 8000 rpm, with 1.0 mm depth of cut

considering hardness of green Ti6Al4V, ~58 HV, which is one fifth of the bulk Ti6Al4V. As the metal particles were embedded in soft polymer matrix, it was relatively easier to remove the material during machining. Notably, there was insignificant heat generation as observed during machining. In connection to this, tool tip utilized for machining operation, nearly 20 h, was examined under SEM microscope. Observation of SEM images revealed insignificant wear on the tool surface due to involvement of insignificant frictional forces. Moreover, it was also noticed that the machined chips were embedded in between diamond particles and were easily cleaned for next job (Fig. 1).

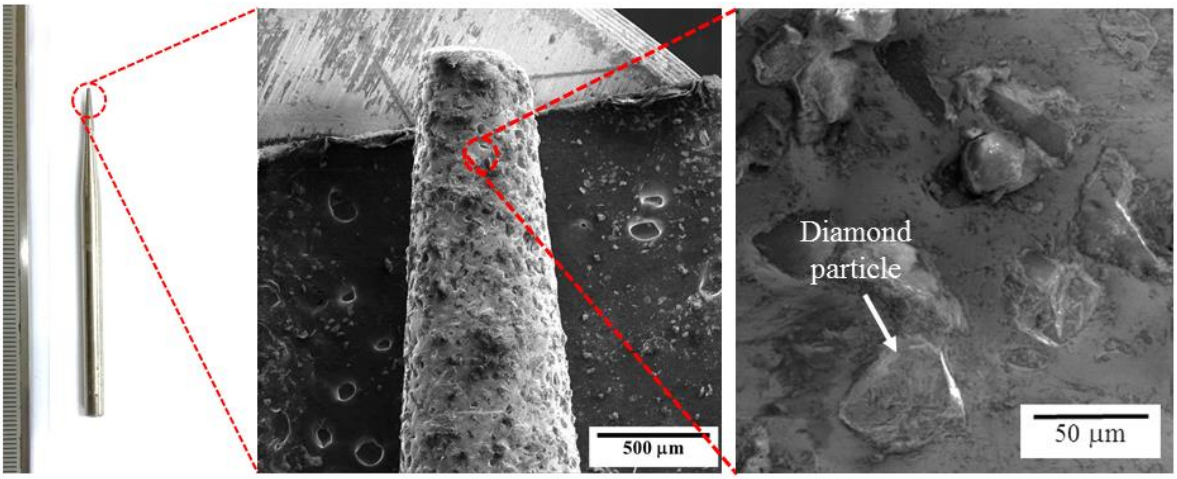

Fig. 1. Tool with higher magnification used for machining green Ti6Al4V

The extruded green Ti6Al4V rod and sheet had similar density; therefore, same parameters were used for machining of both the objects with the prior anticipation of shrinkage. The length of rod was chosen based on optimization of maximum area for machining with minimum vibrational effect during tool movement. The rod was fixed at one end with the help of a sample holder and the other end was supported by tailstock (Fig. 2a). The machining was performed in rotary mode since the model had rotational symmetry. The tool movement direction was selected along the symmetrical axis for absorption of maximum machining stress by the sample holder. As shown in Fig. 2d, material (i.e., Ti6Al4V particle-polymer premix) was

removed through machining leaving a smooth surface finish owing to finer notch [29]. After machining, dental root equivalents were cut from both the ends to get final component (Fig. 2b). Similarly, sample sheet was placed in stationary mode and fixed on machining platform with the help of paper clips. Using similar machining parameters, spinal plate equivalent was successfully machined in green state without any visual surface cracks (Fig. 2c).

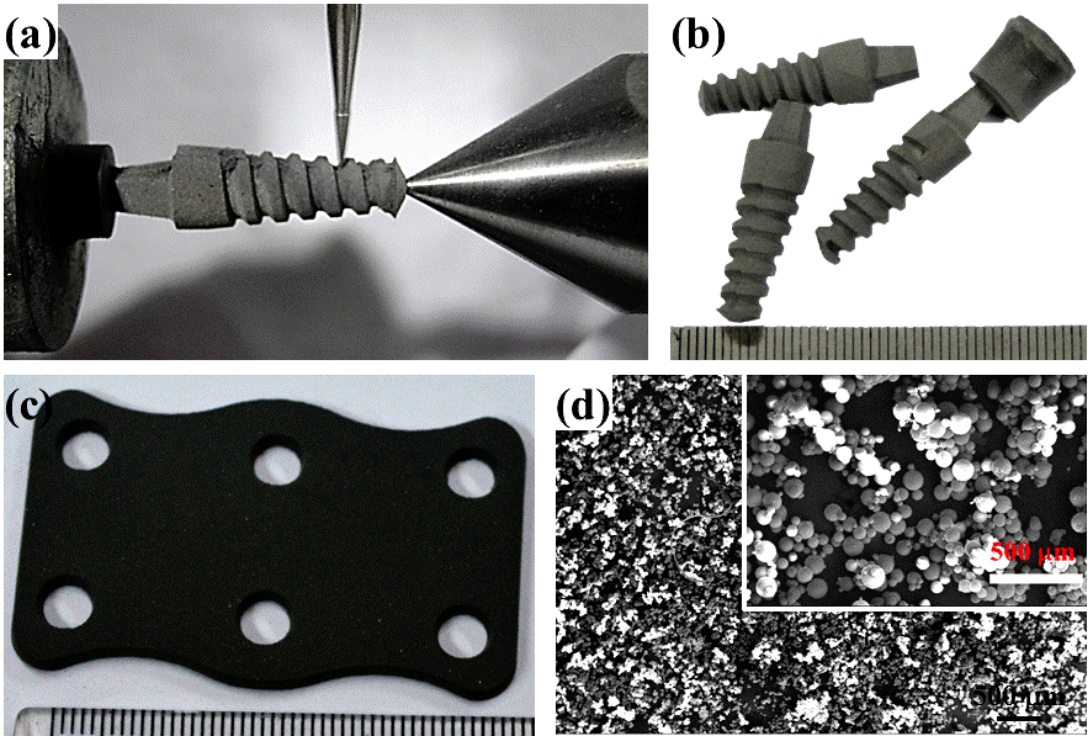

Fig. 2. Optical image of the machined green bodies (a) machining operation of dental root equivalent under rotary mode; (b) machined dental root equivalents and (c) spinal plate equivalent; (d) chips produced during machining of green Ti6Al4V using diamond embedded tool

The dental root and spinal plate equivalents were successfully sintered under inert atmosphere. The sintered root did not show any significant deformation (Fig. 3a); however, the spinal plate was partially deformed, possibly due to high aspect ratio of the sample and variation in Ti6Al4V particle distribution [30]. Machining lines were observed at the edge of the spinal plate due to scooping out of the material during vertical machining along with the conical

geometry and roughness of the diamond-coated tool (Fig. 3b). A thin oxide layer was observed on the sintered samples since the samples were exposed to atmospheric oxygen during machining (Fig. S1 in Supplementary materials). The holes in sintered spinal plate equivalent were elongated diagonally for differential shrinkage through sintering along the length and the width. Further, release of residual stress accumulated during sample preparation during sintering and cooling cycles greatly contributed to the anomalies observed with spinal plate equivalent.

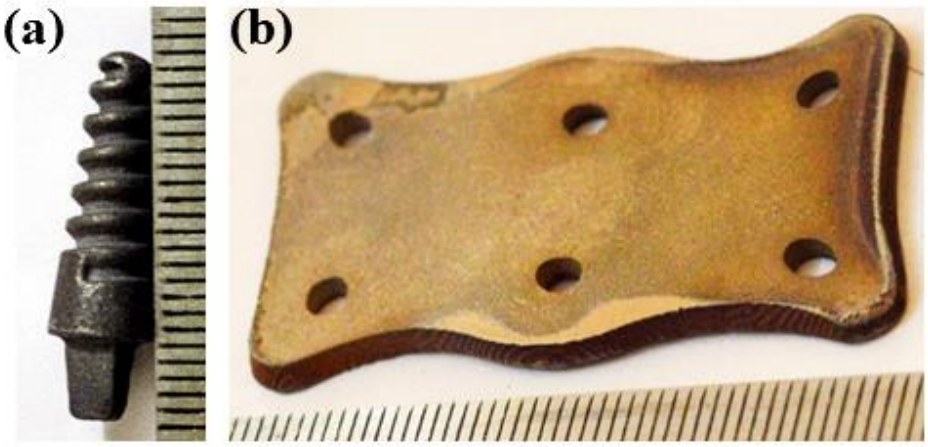

Fig. 3. Optical image of sintered Ti6Al4V implants (a) dental root (b) spinal plate equivalents

2.3 Surface topography and roughness

The surface of the green-machined samples showed uniform particle distribution before and after machining as observed from SEM images (Fig. 4a-b). However, the sinter surface was uneven containing several visual surface defects (Fig. 4c). The machined sintered surface was relatively smoother than that of the as formed ones. This might be due to elastic bounce back of the Ti6Al4V-polymer dough associated with pressure release immediately after the tool shifting to another point. Migration of surface grains without any surface defects was also noted leading to reduction in surface roughness after sintering (Fig. 4d) [31].

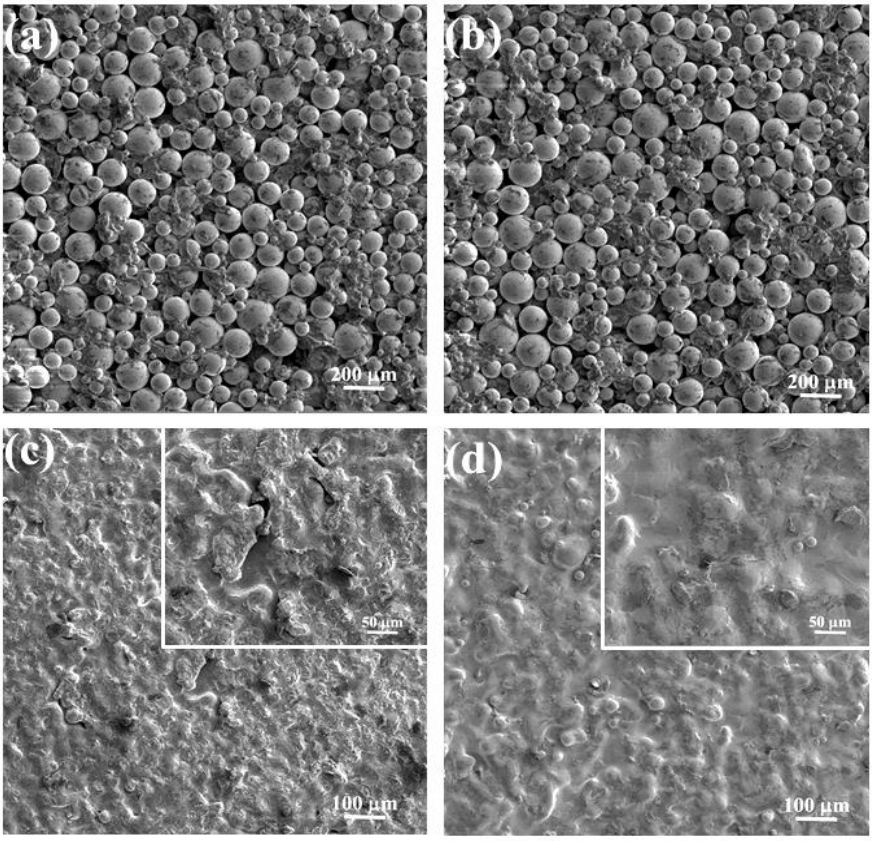

Fig. 4. SEM micrographs of Ti6Al4V sample (a) as prepared green surface, (b) machined green surface, (c) as prepared surface after sintering, (d) machined surface after sintering

The surface roughness of green and sintered Ti6Al4V samples (both as prepared and machined) was quantitatively analyzed. The average value of surface roughness for as prepared green Ti6Al4V was measured to be 11.0 ± 1.2 µm; however, the machined green surface was relatively smooth with an average value of surface roughness to be 10.3 ± 0.4 µm (Fig. 5a-b). Similarly, machined sintered samples showed comparatively smoother surface (13.3 ± 0.3 µm) than virgin sintered Ti6Al4V (14.8 ± 1.4 µm) (Fig. 5c-d).

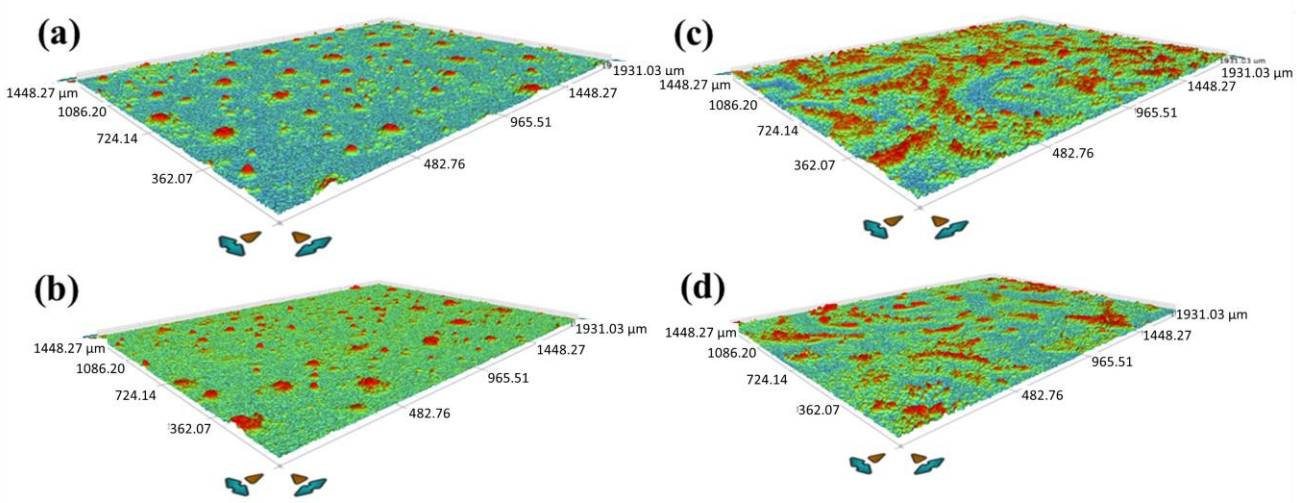

Analytical data from optical surface profilometry

Label (Units)	Values for the samples			
	(a)	(b)	(c)	(d)
Average (µm)	0	0	0	0
Data Points	1239064.064	1239113.984	12343617.024	1241719.04
% Data Points	99.59	99.6	99.96	99.8
R_a (µm)	11.075	10.307	14.777	13.133
R_p (µm)	78.671	73.914	57.641	74.021
R_q (µm)	14.747	13.392	18.126	16.739
R_t (µm)	138.686	136.823	126.109	140.845
R_v (µm)	-60.015	-62.91	-68.468	-66.824

Fig. 5. Optical surface profilometry 3D image and analytical data of (a) as prepared green Ti6Al4V, (b) surface after machining, (c) as prepared sintered Ti6Al4V surface, (d) sintered surface after machining

2.4 Micro-CT

Percentage density and defect sizes of the sintered samples were quantitatively assessed by micro-CT analysis. Both the implants were scanned using the same parameters. The implants were found to have 98.54 ± 3.4% of theoretical density. Notably, the root exhibited large internal defects with the maximum size of 1.48 mm (Fig. 6a-b). Such defects might have originated from the entrapped air bubbles during dough extrusion. However, the spinal plate showed uniform distribution of pores with the maximum pore size of 0.83 mm (Fig. 6c-d). The spinal plate

exhibited comparatively smaller pore size than that of the dental root equivalent. This could be attributed to the difference in their fabrication process. The sheet for spinal plate was prepared from sheets by passing the dough through rollers. Since rolling is an open process, there was less chance of air entrapment into the sheet. In case of root, the dough was first extruded from a closed metallic die to form a rod, in which air entrapment was highly possible.

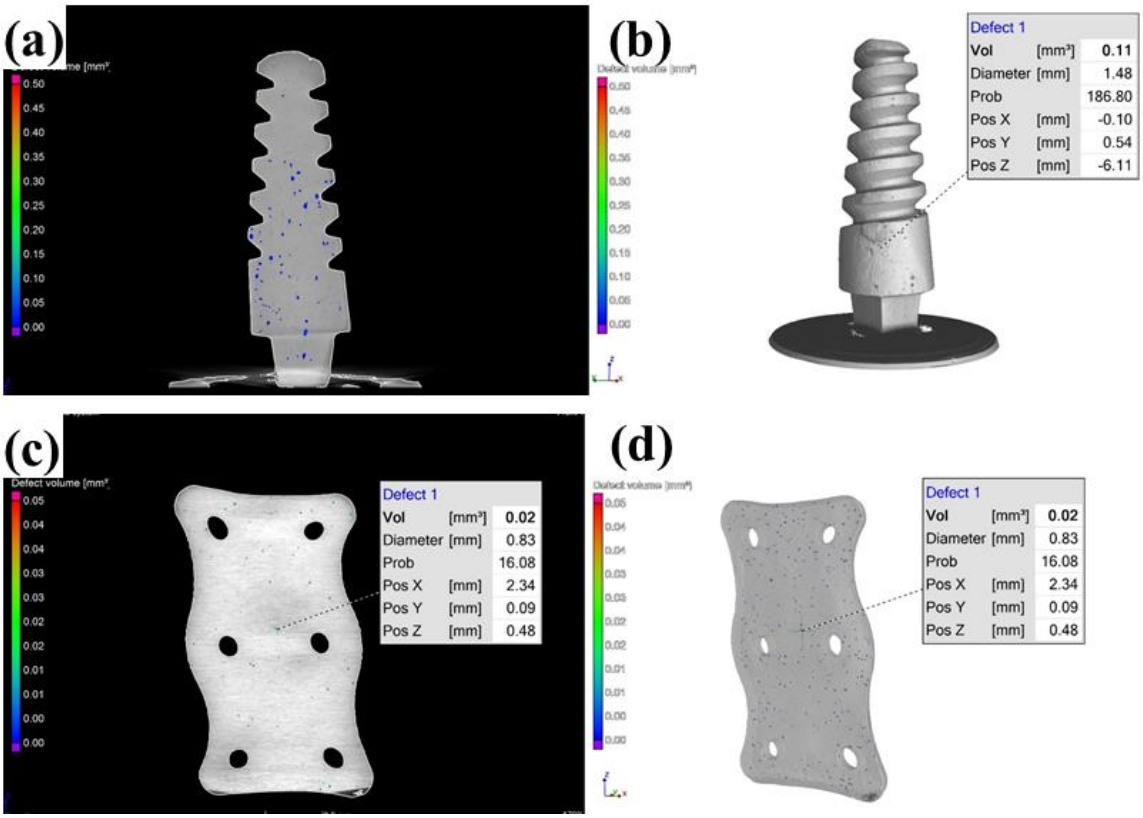

Fig. 6. (a) Cross-sectional 2D view of dental root; (b) isometric view of sintered dental root scanned by micro-CT; (c) cross-sectional view of sintered spinal plate; (d) isometric view of sintered spinal plate scanned by micro-CT

2.5 Anisotropic shrinkage

Anisotropic shrinkage analysis of the machined Ti6Al4V samples was carried out to evaluate feasibility of net shape fabrication of customized implants like dental root and spinal plate by rapid tooling or CNC machining. Dimensional analysis of sintered machined implants showed that there were linear shrinkages of ~15% in all the directions. The shrinkage analysis of

both dental root and spinal plate equivalents using XOV software displayed significant isotropy in all directions as shown in Fig. 7a-b.

2.6 Density distribution

The radiographic image of green and sintered Ti6Al4V sheet acquired through micro-CT was used for analyzing grey value distribution in all the directions. Fig. 7c-d shows the grey value distribution 3D plot corresponding to green and sintered Ti6Al4V. It was noticed that the green Ti6Al4V samples showed grey value variation from one end to other end (Fig. 7c), associated with the variation in X-ray penetration through the powder-binder mixture. However, sintered and machined sintered Ti6Al4V samples exhibited relatively homogenous grey value distribution in all the directions as compared to green one revealing homogeneity of the sample after sintering (Fig. 7d). Notably, no significant difference was observed with unmachined/machined surfaces of green and sintered Ti6Al4V.

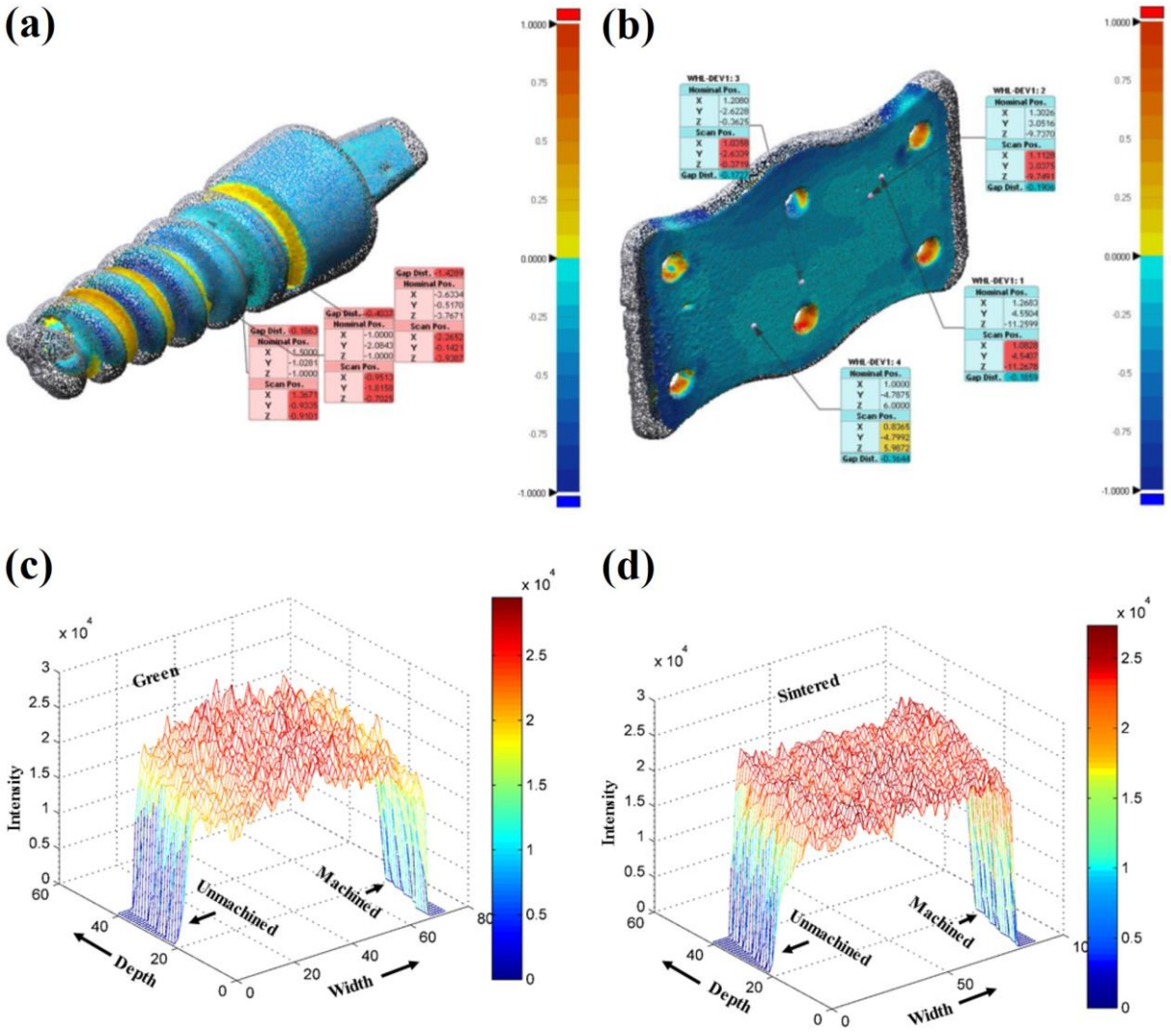

Fig. 7. Comparison of as machined green implants with sintered ones as a result of shrinkage associated with sintering (a) dental root and (b) spinal plate equivalents; 3D plot of grey value distribution from as prepared surface to machined surface for (c) green and (d) sintered Ti6Al4V samples

2.7 Flexural strength

Average flexural strength and flexural modulus out of ten machined sintered samples were estimated to be 774.3 ± 26.2 MPa and 101.8 ± 4.1 GPa, respectively. There was a significant increase in flexural strength for the machined sintered Ti6Al4V in comparison with the original one, similar to our previous study [5]. From the SEM images, it was evident that the

machined Ti6Al4V samples after sintering displayed comparatively smoother surface without visible defects than unmachined sintered samples (Fig. 4a-b). Increase of flexural strength in the machined Ti6Al4V could be correlated with the reduced surface roughness. Since green machining of Ti6Al4V is reported for the first time, the Weibull modulus study was performed to assess the reliability of mechanical properties of the samples for process viability. Weibull modulus calculated from the slope of plot ln(ln(1/Ps)) vs ln σ_{max} was measured to be 27.75 with nearly 96 % confidence interval (Fig. 8a). Significant increase in values of Weibull modulus and confidence interval for the green-machined samples was observed with respect to its virgin samples. From the Weibull modulus value, it may be concluded that the samples prepared by green machining exhibited reliable mechanical properties. Further, SEM analysis of fractured surface of machined sintered sample revealed river line morphology along with dimples confirming that the facture behavior of the sample was brittle and ductile in nature (Fig. 8b).

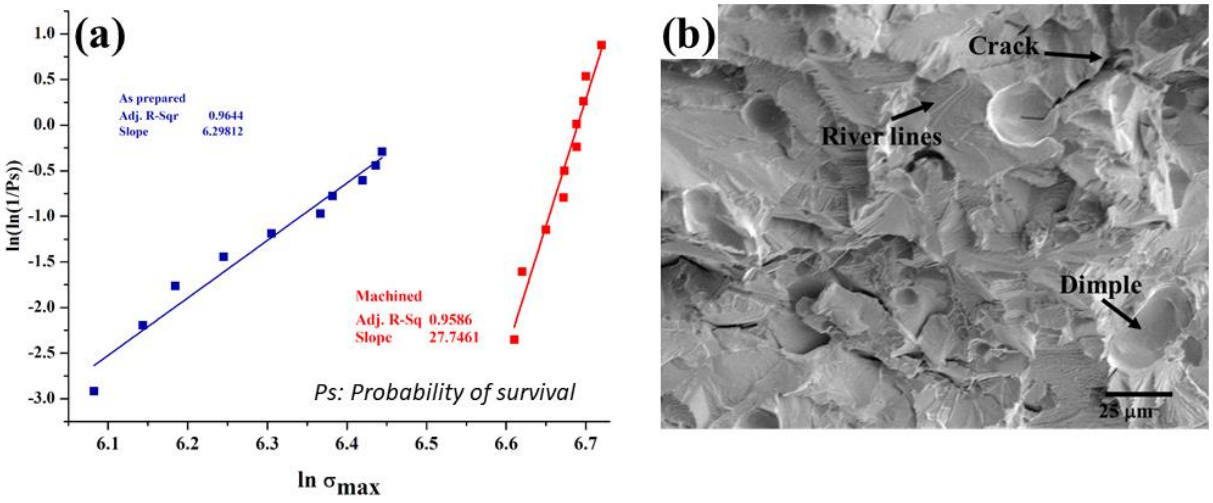

Fig. 8. (a) Weibull distribution plot for flexural strength data of machined sintered Ti6Al4V samples as compared to as prepared Ti6Al4V (red colored line indicates best fitting curve); (b) SEM images of machined sintered fractured Ti6Al4V surface demonstrating brittle and ductile behavior of sample.

3. Conclusion

The study successfully conducted green machining of Ti6Al4V compacts using CNC tooling. The dried green samples, prepared through PDP, were easily machinable into predefined shapes without much difficulty due to the low hardness. The process did not utilize any coolants or costly tool; still, it could produce a smooth machined surface of the final objects without applying high machining force. The custom-designed diamond embedded pointed tool was successfully utilized for machining of fine features with satisfactory dimensional accuracy and surface finish. Moreover, the machined Ti6Al4V samples after sintering exhibited close dimensional accuracy with isotropic linear shrinkage limited to ~15% of the green Ti6Al4V samples. The average flexural strength and flexural modulus were found to be 774.3 ± 26.2 MPa and 101.8 ± 4.1 GPa, respectively, as applicable for load-bearing application. Weibull modulus study further validated the process reliability based on mechanical properties of the samples. The similar samples produced by PDP tested for in vitro cytotoxicity and human mesenchymal stem cell (hMSC) response supported cytocompatibility with high osteogenic potential, as evident in another study by the author [33]. However, due to the limited scope, biological data were excluded from this study. Overall, the study concludes that green machining could be an alternative for developing titanium-based implants.

4. Materials and Methods

4.1 3D design of Ti6Al4V implant

The CAD (Computer Aided Design) models of biomedical implants were developed using Solidworks® (Dassault Systèmes SOLIDWORKS Corp., USA) and converted into ‘stl’ format (as shown in Fig. 11). Prior to green machining, ‘stl’ formats were selected to develop

near net shaped objects resembling a dental root and a spinal plate. A 4-axis desktop CNC machine (MODELA pro, MDX-540) was employed for green machining of machinable green Ti6Al4V compacts fixed on either stationary or rotary platform.

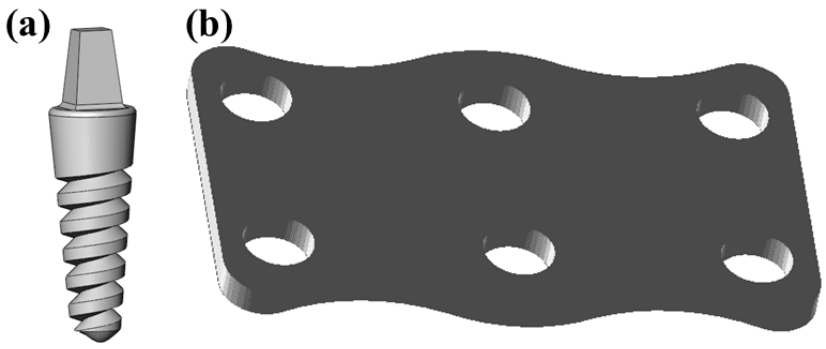

Fig. 9. Isometric view of 3D CAD implant models (a) dental root, (b) spinal plate

4.2 Dough Preparation and shape prefabrication

Ti6Al4V green compacts were prepared by an optimized procedure, i.e., plastic dough process (PDP) reported elsewhere [5, 6]. Briefly, a blend was prepared in a beaker by premixing of Ti6Al4V powders (particle size 15–45 μm) in required quantity with 3 wt% chitosan as binder, 1 wt% glycerol as plasticizer, 1 wt% stearic acid as lubricant and 13 wt% of 40% v/v aqueous acetic acid as solvent for dissolving chitosan. The blend was subjected to high shear mixing for ~ 30 min at 10 ^{o}C to convert into a high viscous dough with constitutional homogeneity and removal of entrapped air bubbles. The dough was plastically deformed into rods and sheets, followed by vacuum drying at room temperature to minimize surface oxidation. Consequently, Ti6Al4V dried green samples were obtained.

4.3 Tool design and green machining

Based on previous studies, diamond embedded pointed tool was chosen for milling green Ti6Al4V [27]. All the tools used for machining green bodies were custom designed through a

metal deposition process, electrolysis, where diamond particles of varied sizes were embedded on the SS metal blank. Variation in tool roughness was due to up projection of diamond particles of varied sizes. The diamond particles embedded on the metal shank provided surface roughness for indentation and scooping out materials from the workpiece. A 4-axis desktop CNC milling machine (MDX 540, Roland DG Ltd., Japan) controlled by software (MODELA 4, Japan) was used for machining of Ti6Al4V dried green samples. The dried shapes were mechanically mounted on the CNC machine table. The 'stl' file of implants was imported in MODELA software for tool path generation and optimizing machining parameters. Machining parameters such as spindle rpm, X-Y-Z linear movement, depth of cut, tool path, path interval *etc*. were optimized based on physico-mechanical characteristics of green body. The optimized machining parameters were used for roughing and finishing purpose.

4.4 Sintering of machined green samples

The fully dried dental roots and spinal plate equivalents were transferred to an alumina tube furnace (Bysakh and Company, Kolkata, India) and kept under argon atmosphere. Before sintering of the samples, the polymeric binder and other organic components were successfully removed by heating at 600 ^{o}C for 3 h at heating rate of 1 ^{o}C/min and finally sintered at 1400 ^{o}C for 8 h at the same heating rate.

4.5 Sample characterization

4.5.1 Surface topography and roughness

The machined Ti6Al4V samples were examined under scanning electron microscope (ZEISS EVO 60 Scanning Electron Microscope, Germany) for surface topography. The surface texture of the as prepared green sample, machined green and as sintered samples as well as machined sintered sample were assessed under Bruker contour GT-X 3D optical microscope.

4.5.2 Micro-CT

The machined green and sintered samples were analyzed by micro-CT based 3D Imaging System (GE phoenix v|tome|x, Germany) using X-ray source voltage 170 kV, beam current 95 mA, scanning resolution 29 µm and 0.5 mm copper filter, for evaluation of internal defects and total density. Additionally, qualitative and quantitative shrinkage analysis was carried out from the corresponding 3D scanned image data using VGStudio MAX (Volume Graphics, Germany) software.

4.5.3 Anisotropic shrinkage

Shrinkage associated with sintering causes reduction in size of green-machined objects. An unpredictable shrinkage may lead to deviation in shape and size of the final product. Shrinkage study was performed between machined green and sintered implants for quantitative evaluation. This study was necessary to validate the close-fit of the fabricated Ti6Al4V implants to the desired ones after sintering. Conventionally, the percent shrinkage during drying and sintering was calculated using linear dimensional measurements of the objects. Further, the nature of shrinkage in unsymmetrical objects like dental root and spinal plate was studied by micro-CT based 3D imaging and comparing the data obtained before and after sintering through reverse engineering tool like ‘XOV’ software. This analysis is important to understand and assess nature of shrinkage, isotropic or anisotropic, associated with sintering.

4.5.4 Density distribution

Density distribution for green and sintered Ti6Al4V samples were analyzed through measurement of voxel value distribution in micro-CT images for green and machined samples. Three-dimensional (3D) X-ray images were acquired by micro-CT for both green and sintered samples and analyzed for voxel value using MATLAB.

4.5.5 Flexural strength

The flexural strength of machined sintered samples was measured by three-point bending test using a Universal Testing Machine (UTM) (Hounsfield, Model H25KS, Redhill, England) with a gouge length of 25 mm, at a crosshead speed of 1.0 mm/min. Ten samples were cut from machined sintered sheet for testing and average flexural strength value was reported.

Acknowledgements

This study was financially supported by Defence Research and Development Organization (DRDO) (Grant no. DLS/81/48222/LSRB-241/BDB/2012), Government of India, BIRAC SRISTI, and the Department of Biotechnology (DBT) (grant no. BIRAC SRISTI PMU-2016/004). Authors also acknowledge Central Research Facility (CRF), IIT Kharagpur for providing facilities of materials characterization.

Conflict of Interest

Authors have no conflict of interest.

Authors' contributions

P.K.S. designed the experiments; P.K.S., K.K. and KC performed experiments, analyzed data with S.K.; P.K.S. drafted the manuscript; K.K., B.S and S.D. evaluated the results and corrected the manuscript; All authors reviewed the results and approved the final version of the manuscript.

References

[1] K. Kapat, P.K. Srivas, A.P. Rameshbabu, P.P. Maity, S. Jana, J. Dutta, P. Majumdar, D. Chakrabarti, S. Dhara, ACS applied materials & interfaces, 9 (2017) 39235-39248.

[2] K. Kapat, P.P. Maity, A.P. Rameshbabu, P.K. Srivas, P. Majumdar, D. Chakrabarti, S. Dhara, Journal of Materials Chemistry B, 6 (2018) 2877-2893.
[3] Z.Z. Fang, J.D. Paramore, P. Sun, K.R. Chandran, Y. Zhang, Y. Xia, F. Cao, M. Koopman, M. Free, International Materials Reviews, 63 (2018) 407-459.
[4] K. Kapat, P.K. Srivas, S. Dhara, Materials Science and Engineering: A, 689 (2017) 63-71.
[5] P.K. Srivas, K. Kapat, M. Wan, S. Dhara, Journal of Manufacturing Science and Engineering, 140 (2018) 071014.
[6] P.K. Srivas, K. Kapat, S. Dhara, U.S. Patent Application 10/022,792, 2018.
[7] R. Khettabi, L. Fatmi, J. Masounave, V. Songmene, CIRP Journal of Manufacturing Science and Technology, 6 (2013) 175-180.
[8] F. Wang, Y. Liu, Y. Zhang, Z. Tang, R. Ji, C. Zheng, Journal of Materials Processing Technology, 214 (2014) 531-538.
[9] A. Zareena, S. Veldhuis, Journal of Materials Processing Technology, 212 (2012) 560-570.
[10] A. Hosseini, H.A. Kishawy, Cutting tool materials and tool wear, Machining of Titanium Alloys, Springer, 2014, pp. 31-56.
[11] S. Honghua, L. Peng, F. Yucan, X. Jiuhua, Chinese Journal of Aeronautics, 25 (2012) 784-790.
[12] M. Balažic, J. Kopać, Strojniski Vestnik/Journal of Mechanical Engineering, 56 (2010).
[13] J. Hughes, A. Sharman, K. Ridgway, Proceedings of the Institution of Mechanical Engineers, Part B: Journal of Engineering Manufacture, 220 (2006) 93-107.
[14] J. Sun, Y. Guo, Journal of Materials Processing Technology, 209 (2009) 4036-4042.
[15] E.M. Trent, P.K. Wright, Metal cutting, Butterworth-Heinemann, 2000.
[16] G. Barrow, CIRP, l 973, 22,(2), 203-2 ll, (1974).
[17] A. Pramanik, The International Journal of Advanced Manufacturing Technology, 70 (2014) 919-928.
[18] Z. Wang, E. Ezugwu, A. Gupta, Tribology transactions, 41 (1998) 289-295.
[19] S. Lei, W. Liu, International Journal of Machine Tools and Manufacture, 42 (2002) 653-661.
[20] J.P. Davim, Machining of titanium alloys, Springer, 2014.
[21] P. Dearnley, A. Grearson, Materials Science and Technology, 2 (1986) 47-58.
[22] Z. Zoya, R. Krishnamurthy, Journal of Materials Processing Technology, 100 (2000) 80-86.

[23] A.N. Amin, A.F. Ismail, M.N. Khairusshima, Journal of Materials Processing Technology, 192 (2007) 147-158.

[24] A. Pramanik, M. Islam, A. Basak, G. Littlefair, Advanced Materials Research, Trans Tech Publ, 2013, pp. 338-343.

[25] R. M'saoubi, J. Outeiro, B. Changeux, J. Lebrun, A.M. Dias, Journal of materials processing technology, 96 (1999) 225-233.

[26] R. Kamboj, S. Dhara, P. Bhargava, Journal of the European Ceramic Society, 23 (2003) 1005-1011.

[27] S. Mohanty, A.P. Rameshbabu, S. Dhara, Ceramics International, 39 (2013) 8985-8993.

[28] P.K. Srivas, K. Kapat, M. Wan, S. Dhara, Journal of Manufacturing Science and Engineering (2018) 071014.

[29] P. Dadhich, P.K. Srivas, S. Mohanty, S. Dhara, Journal of the European Ceramic Society, 35 (2015) 3909-3916.

[30] C. Jamin, T. Rasp, T. Kraft, O. Guillon, Journal of the European Ceramic Society, 33 (2013) 3221-3230.

[31] P.P. Nampi, S. Kume, Y. Hotta, K. Watari, Bulletin of Materials Science, 34 (2011) 799-804.

[32] P.K. Srivas, K. Kapat, B. Das, P. Pal, P.G. Ray, S. Dhara, Applied Surface Science, 478 (2019) 806-817.